Journal of Spatial Information Sciences

... JSIS



MAPPING NIGER DELTA FLOOD DYNAMICS VIA MULTI-TEMPORAL SAR INTENSITY AND COHERENCE FUSION

LEONARD M.O AMINIGBO, OLUDAYO E. ABIODUN,
OLUSOLA G. OMOGUNLOYE



JOURNAL OF SPATIAL INFORMATION SCIENCES ISSN: 2354-3361
VOL. 3, ISSUE 2, PP 58–83, 2026 PUBLISHED 24-11-2026
www.journals.unizik.edu.ng/jsis

MAPPING NIGER DELTA FLOOD DYNAMICS VIA MULTI-TEMPORAL SAR INTENSITY AND COHERENCE FUSION

Leonard M. O. Aminigbo[1*], Oludayo E. Abiodun[2], Olusola G. Omogunloye[2]

[1]Department of Geography & Environment, Rivers state University, Nkoplu-Orowokwu Port Harcourt
[2]Department of Surveying & Geoinformatics, University of Lagos, Akoka Lagos

Email: leonard.aminigbo@ust.edu.ng, oabiodun@unilag.edu.ng

Phone numbers: 08030899971, 08066513914

Abstract

The geographic scope of this research focuses on parts of the Niger Delta region of Nigeria, specifically focusing on critical hydrological catchments and urban centers across Bayelsa, Delta, and Rivers states. The region is bounded by the Atlantic Ocean to the south and is topographically characterized by an extensive, low-lying alluvial plain with elevation gradients primarily ranging from -6 m to 22 m above mean sea level.

The Niger Delta region of Nigeria faces escalating flood risks driven by the convergence of natural vulnerability and intensive anthropogenic pressures[4]. This study utilized the Sentinel-1 Synthetic Aperture Radar (SAR) dataset to overcome the limitations of persistent cloud cover during the peak monsoon season. A Multi-temporal Sentinel-1 Intensity and Interferometric Coherence Fusion Framework was established by combining SAR backscatter with repeat-pass interferometric coherence layers to distinguish open water from flooded vegetation.

Though the C-band (~5.6 cm) SAR dataset provides great temporal frequency, it has limited canopy penetration compared to L-band sensors (like ALOS-2 or NISAR), which are inherently better suited for sub-canopy wetland mapping. However, while L-band is ideal, the fusion of Interferometric Coherence with backscatter intensity mathematically compensates for C-band's limitations by detecting decorrelation in flooded vegetation.

Data acquisition spanned a multi-year temporal series between (2017–2025) to map active seasonal inundation footprints.

Spatio-temporal analysis showed that flood extents in key areas like Yenagoa expanded by 64% between 2017 and 2021, primarily affecting low-lying zones with elevations between -6 m and 7 m. Furthermore, the findings showed that emergency water releases from upstream dams, such as Lagdo and Jebba, significantly exacerbate downstream inundation during peak monsoon periods. The study highlights the critical role of all-weather SAR sensors in overcoming the atmospheric limitations of cloud-heavy tropical climates. Ultimately, the results advocate for an integrated resilience framework that combines Hybrid AI-Integrated Modeling with stricter environmental regulation and community-based land management to mitigate future humanitarian and socio-economic crises.

Keywords: Niger Delta, Flood Dynamics, Sentinel-1, SAR, Coherence Fusion, Multi-temporal.

1.0: Introduction

The Niger Delta region of Nigeria constitutes one of the most complex and ecologically significant deltaic systems in the world, serving as the terminal basin for the Niger River, which traverses thousands of kilometers across West Africa before discharging into the Atlantic Ocean through a dense network of distributaries and estuaries. Occupying a significant portion of Nigeria's coastal zone, this landscape is characterized by a fragile geological equilibrium between riverine hydraulic forces and coastal marine processes. Over the last four decades, however, the region has transitioned from a naturally resilient wetland system into a high-risk environment where flood events have become increasingly frequent, severe, and unpredictable. Consequently, the mapping of these spatio-temporal dynamics is not merely a technical exercise in hydrology but a critical requirement for the protection of millions of inhabitants whose lives, livelihoods, and critical infrastructure are under constant threat from the dual pressures of inland riverine discharge and oceanic sea-level rise. The core challenge facing the Niger Delta is a compounding socio-environmental cycle where rapid human expansion directly undermines natural flood defenses. While flooding is inherently a natural phenomenon driven by the region's low topography, high annual rainfall, and tidal surges, human activities have significantly exacerbated these baseline risks. Uncontrolled urban sprawl has seen settlements increase dramatically with residential and industrial structures systematically creeping into wetlands and mangrove forests, thereby reducing the ecosystem's natural capacity to absorb and attenuate floodwaters [10]. Furthermore, the proliferation of oil and gas infrastructure, such as pipelines and flow stations, frequently interferes with natural hydrological patterns, acting as physical barriers that cause upstream water accumulation and localized inundation. This intersection of natural vulnerability and structural governance failure has resulted in catastrophic socio-economic impacts, leading to the recurrent destruction of agricultural livelihoods [12]. Despite the increasing frequency of these disasters, critical gaps remain in the current body of technical knowledge regarding flood management in the Niger Delta. The majority of existing land-use and flood mapping studies rely heavily on optical sensors, which are severely limited by persistent cloud cover and high humidity in the tropical Niger Delta climate [14]. This atmospheric interference leads to significant noise in datasets and severe temporal gaps during the peak rainy season precisely when accurate mapping is most critical.

To address these limitations, this study utilizes multitemporal Sentinel-1 Synthetic Aperture Radar (SAR) to delineate and quantify the spatio-temporal intensity and optical imagery filtered for cloud-free windows (cloud cover $< 10\%$) to compute vegetation indices (NDVI, $CI_{red\text{-}edge1}$) and establish baseline crop boundary masks. and distribution of flood. By assessing the multi-temporal impacts of land use change, upstream dam operations, and relative sea-level rise, this research establishes a foundational framework for climate-resilient planning and disaster management in high-risk deltaic catchments [1].

2.0: Geological, Hydrological, and Anthropogenic Drivers of Flooding

2.1 Topographic and Hydrological Baselines

The geomorphological evolution of the Niger Delta is driven by a delicate balance between the rate of sediment supply from the Niger-Benue river system and the rates of baseline subsidence and oceanic removal[7]. This process has historically created a vast alluvial basin characterized by extremely low relief across three primary ecological zones: barrier islands, mangrove swamp zones, and freshwater swamp forests [4].

The hydrology of this network is dominated by the River Niger, which splits into the Nun and Forcados rivers within 100 to 120 kilometers of the coast, branching further into a braided matrix of rivers and creeks [16].

Table 2: Comparative Suitability of SAR Bands for Niger Delta Monitoring

SAR Band/Sensor	Wavelength (Approx.)	Vegetation Penetration	Flood Mapping (Vegetated)	Crop Structure Retrieval (RVoG)	Significance for Niger Delta
Sentinel-1 (C-band)	5.55 cm	Low	Medium (Surface scattering)	Limited (Only top canopy)	Insufficient for sub-canopy inundation mapping or DTM generation.
ALOS 2/NISAR (L-band)	24 cm	High (Stem/Ground)	Superior (Double-bounce detection.	High (Effective for	Optimal Choice: Required for high-accuracy

				Height/Biomass)	
TanDEM-X (X-band)	3.1 cm	Very Low	Low	High (But only for sparse/short canopy)	Impractical for dense tropical agricultural settings like the Niger Delta.

The region's hydrological regime is governed by the annual cycle of the Niger River, which experiences two distinct flood peaks: the white flood and the black flood. The white flood, characterized by low sediment content, arrives between July and October following the rainy season in the middle Niger catchment. Conversely, the black flood, bearing higher sediment concentrations from the upper Niger, typically reaches the delta in December [2].

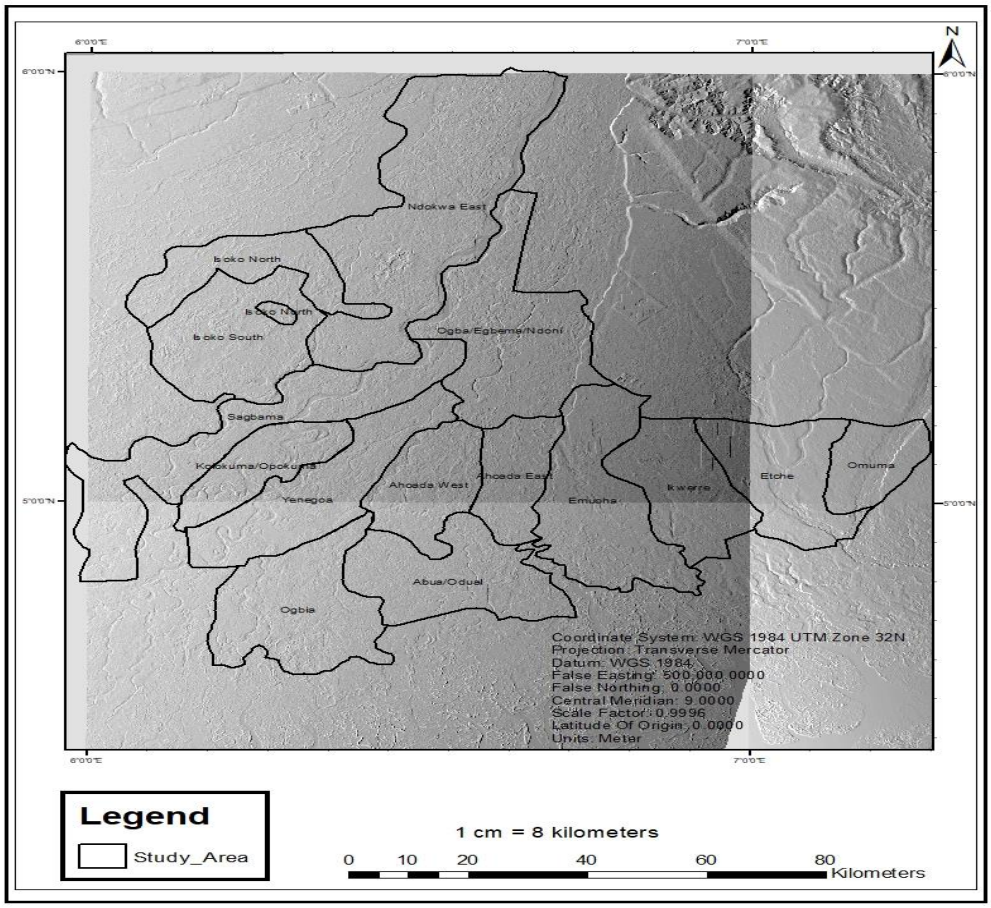


Fig. 1: Synthetic Aperture Radar Image Map of 16 Local Government Areas of the Niger Delta.

Because the Benue River has a more southerly location and a single high-water season from May to October, its confluence at Lokoja ensures that the lower Niger maintains a prolonged high-water period and a significantly shortened low-water season. During these peak periods, water levels can rise substantially, fundamentally altering the delta's low-lying landscape [13].

2.2: The Influence of Upstream Dam Operations

The impoundment of multiple large dams within the Niger catchment area has fundamentally altered natural streamflow and sediment delivery to the coast. Hydrograph simulations demonstrate a clear delayed downstream response to water releases from the Kainji and Jebba dams in Nigeria, as well as the Lagdo Dam in Cameroon[11]. While these reservoirs are designed for hydropower and irrigation, emergency water releases during peak monsoon periods routinely overwhelm downstream floodplains. Furthermore, these dams trap sediment that would naturally replenish the delta, causing riverbeds to erode and rendering riverine communities increasingly vulnerable to bank overtopping.

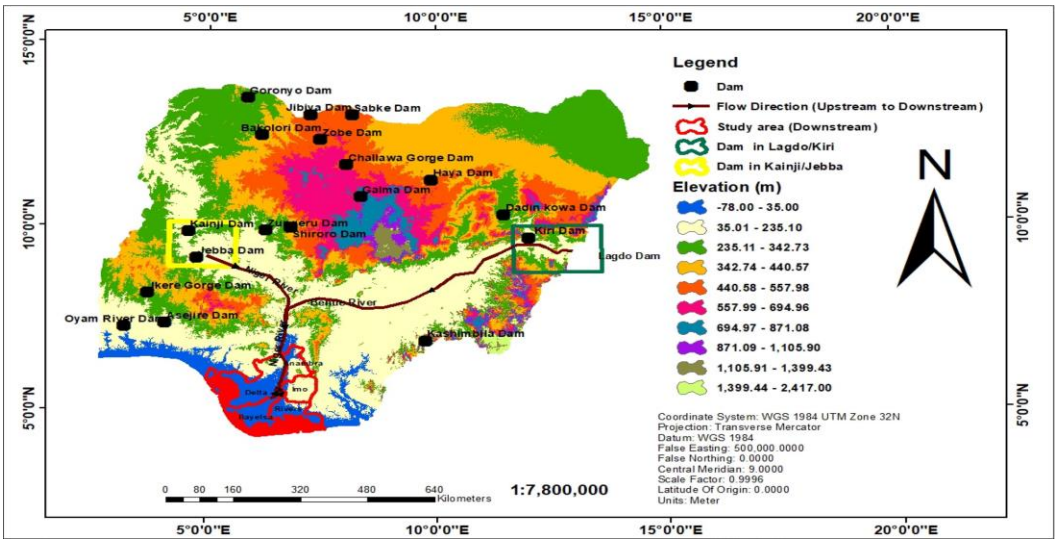


Fig. 2: Map of upstream dams in Nigeria (Source: Eteh, Japheth, Akajiaku, Osondu · Mene-Ejegi, Oriasi, Omietimi, and Ayo-Bali., 2025).

2.3: Coastal Vulnerability and Sea-Level Rise

Compounding these riverine risks is the vulnerability of the delta's southern oceanic boundary. Unlike geologically stable coastlines, the Niger Delta is a subsiding basin, meaning that its relative sea-level rise (SLR) is much higher than global averages [5].

Because upstream dams have reduced sediment delivery by 70%, the delta can no longer geomorphologically replenish itself as it sinks. According to the Coastal Vulnerability Index (CVSLRI), which evaluates 17 physical and social indicators, approximately 67% of the 500 km coastline exhibits high to very high vulnerability. Shoreline dynamics are in a state of volatile flux, with severe erosion hotspots like Escravos, Forcados, and Brass experiencing historical erosion rates up to 18 m/year.

3.0: Materials and Methods

The geographic scope of this research focuses on parts of the Niger Delta region of Nigeria, specifically focusing on critical hydrological catchments across Bayelsa, Delta, and Rivers states. The specific administrative sub-units evaluated across the three target states falls within 16 Local Government Areas (LGAs) such as Rivers State; Ahoada West, Ahoada East, Ogba/Egbema/Ndoni (Omoku), Ikwerre, Abua/Odual, Emohua, Etche, and Omuma, Bayelsa State; Yenagoa, Sagbama, Kolokuma/Opokuma, and Ogbia, Delta State; Ndokwa East, Isoko North, Isoko South, and Patani. The region is bounded by the Atlantic Ocean to the south and is topographically characterized by an extensive, low-lying alluvial plain with elevation gradients primarily ranging from -6 m to 22 m above mean sea level.

Characterized by a tropical monsoon climate, the study area experiences prolonged wet seasons peaking between May and October, with average annual rainfall heavily driving regional streamflow dynamics[18]. The complex network of distributaries, including the Nun and Forcados rivers and the low-relief Orashi River Basin, creates a geomorphological sink highly susceptible to both riverine overbank discharge and marine tidal backwater effects [16].

The following catchment basins were delineated for this study

1. Yenagoa Catchment: Located along the central deltaic axis in Bayelsa State at 4°55′N, 6°15′E and Low-lying urban and agricultural catchment along the Nun River distributary.
2. Warri Metropolitan Area: Located along the western delta corridor in Delta State at 5°31′N, 5°45′E and highly urbanized, estuarine coastal layout characterized by high effective impervious cover.

3. Lower Orashi River Basin: Located along the low-gradient fluvial trough running parallel to the main Niger River stem, spanning approximate coordinates of 4°15′N to 5°45′N and 6°00′E to 7°15′E and encompasses key agrarian LGAs including Ahoada West, Ahoada East, Ogba/Egbema/Ndoni, Abua/Odual, and Ndokwa East. Characterized by minimal slopes (1° to 4°) and poor subsoil permeability.

3.2 Data Acquisition

This study utilized the Sentinel-1 Synthetic Aperture Radar (SAR) dataset to overcome the limitations of persistent cloud cover during the peak monsoon season. A Multi-temporal Sentinel-1 Intensity and Interferometric Coherence Fusion Framework was established by combining SAR backscatter with repeat-pass interferometric coherence layers to distinguish open water from flooded vegetation. Data acquisition spanned a multi-year temporal series (2017–2025) to map active seasonal inundation footprints.

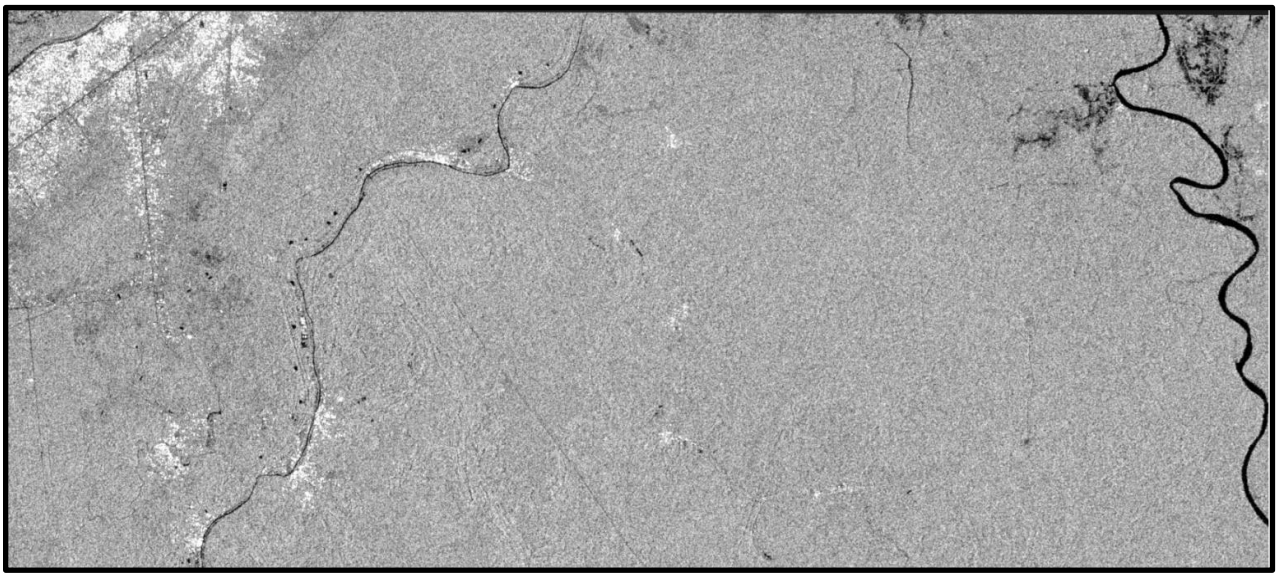


Fig. 3.1: Sentinel-1 C-band (~5.55 cm wavelength) Single Look Complex (SLC) products in Interferometric Wide (IW) swath mode Image dataset covering the study, Area.

The primary datasets integrated into this research include:

1) **Sentinel-1 SAR:** C-band Synthetic Aperture Radar (SAR) imagery captured in the Interferometric Wide (IW) swath mode as Single Look Complex (SLC) products in Interferometric Wide (IW) swath mode. The data features a spatial resolution of 10 meters and utilizes dual-polarization (VV + VH) configurations.

2) **Topographic and Geomorphological Data:** Digital Elevation Models (DEM) sourced from the Shuttle Radar Topography Mission (SRTM) at a 30-meter resolution, supplemented by global TanDEM-X data to resolve vertical terrain discrepancies in low-lying zones.
3) **Auxiliary Data:** Localized monthly rain-gauge data (expressed in mm) used to analyze the rainfall-inundation correlation matrix, alongside field validation points captured via handheld Global Positioning System (GPS) receivers during active field campaigns.

Though the C-band (~5.6 cm) SAR dataset provides great temporal frequency, it has limited canopy penetration compared to L-band sensors (like ALOS-2 or NISAR), which are inherently better suited for sub-canopy wetland mapping. However, while L-band is ideal, the fusion of Interferometric Coherence with backscatter intensity mathematically compensates for C-band's limitations by detecting decorrelation in flooded vegetation.

3.2.1: Technical Specifications

1. Correct Input Product Type & Sensor Details;

a) Required Product Type: Sentinel-1 C-band (~5.55 cm wavelength) Single Look Complex (SLC) products in Interferometric Wide (IW) swath mode.

b) Polarizations Used: Dual-polarization VV (single co-polarization) and VH (cross-polarization).

2. Acquisition Dates, Orbit & Baseline Geometry;

a) Observation Window: Multi-temporal repeat-pass series across the 2017–2025 monsoon cycles (peaking August–October).

b) Orbit Configuration: Relative orbits (ascending or descending passes) maintaining exact frame/swath alignment.

c) Temporal Baseline (Δt): 6 to 12 days (achieved via Sentinel-1A and Sentinel-1B constellation repeat passes).

d) Perpendicular Baseline ($B_\perp$): Small spatial baselines ($|B_\perp| < 100$ m) to minimize spatial decorrelation across tropical wetland target areas.

3. Standard InSAR Coherence Processing Workflow

Interferometric coherence (γ) is defined mathematically as the normalized complex cross-correlation between two co-registered complex images S_1 and S_2:

$$\gamma = \frac{|\sum_{i=1}^{L} S_1(i) S_2^*(i)|}{\sqrt{\sum_{i=1}^{L} |S_1(i)|^2 \sum_{i=1}^{L} |S_2(i)|^2}} \quad \text{.....Equation (1)}$$

where S denotes the complex conjugate and L represents the spatial multi-looking window size (number of looks).

3.2: Data Pre-processing Workflow

To mathematically compensate for the penetration limitations of C-band SAR in dense tropical wetlands, a Multi-temporal Sentinel-1 Intensity and Interferometric Coherence Fusion Framework was developed. This framework blends radar backscatter intensity with repeat-pass interferometric coherence layers to detect decorrelation patterns caused by water beneath vegetation canopy.

3.3: Data Processing Framework

Orthorectification of the imagery using the SRTM 30m DEM was executed to correct for distortions caused by terrain relief, such as foreshortening and layover, projecting the final output onto the WGS84 ellipsoid.

To delineate surface flood dynamics across the complex wetland matrix, a machine learning advanced classification framework was implemented using the Random Forest (RF) algorithm. The multi-dimensional input feature stack compiled for the RF model comprised seven core predictors derived from the pre-processed geospatial data:

(i. Sentinel-1 VV backscatter intensity.
(ii. Sentinel-1 VH backscatter intensity.
(iii. Multi-temporal repeat-pass interferometric coherence layers
(iv. Topographic elevation derived from the SRTM DEM
(v. Surface slope angles derived from TanDEM-X data
(vi. Distance-to-stream proximity vectors
(i. The Topographic Wetness Index (TWI)

The RF classifier hyper-parameters were systematically optimized to ensure stability and mitigate over-fitting. The final model configuration was trained using N estimators = 300 independent decision trees, with the number of features considered at each split point set to the square root of total predictors. Node splitting was governed by Gini impurity criteria, and a minimum leaf size of 2 was maintained to preserve local spatial variations. The generated classification outputs are presented in figures 3.1 through 3.6.

To overcome the severe limitations of persistent cloud cover and atmospheric interference that degrade optical satellite sensors during the peak tropical monsoon season, the study selected active

microwave Synthetic Aperture Radar (SAR) datasets. The primary SAR data source comprised Sentinel-1 C-band imagery as Single Look Complex (SLC) products captured in Interferometric Wide (IW) swath mode. The Sentinel-1 dataset features a 10-meter spatial resolution and utilizes dual-polarization (VV + VH) configurations. Although C-band radar (~5.55 cm wavelength) possesses lower canopy penetration capabilities compared to long-wavelength L-band sensors (such as ALOS-2 or NISAR), the temporal frequency of Sentinel-1 provides ideal multi-year monitoring across the 2017–2025 epoch.

Processing Steps:

1. Precise Orbit Application: Update orbit state vectors using Sentinel-1 Precise Orbit Determination (POD) files.
2. Co-registration: Fine co-registration of reference (master) and secondary (slave) SLC pairs to sub-pixel accuracy using an external Digital Elevation Model (Copernicus DEM / SRTM 30m) and precise orbit metadata.
3. TOPS Debursting & Merging: Seamlessly merge IW sub-swaths and bursts.
4. Coherence Estimation: Generate coherence maps using a spatial multi-look window in a 19×4 boxcar kernel in range/azimuth to balance spatial resolution with phase noise suppression.
5. Topographic Phase Removal (Flat-Earth Removal): Subtract reference topographic phase using the DEM.
6. Terrain Correction & Geocoding: Range-Doppler terrain correction to orthorectify outputs to WGS 84 / UTM Zone 32N at 10 m spatial resolution.

4. Software Environment

a) Primary Engines: ESA SNAP (Sentinel Application Platform) Toolbox / ISCE2 / GMTSAR for SLC-based InSAR processing.

b) Cloud Platform: Google Earth Engine (GEE) or Python API for downscaling, multi-temporal stacking, and machine learning model integration.

5. Coherence Intensity Fusion & Sub-Canopy Detection Procedure

To accurately isolate sub-canopy surface water beneath tropical vegetation:

a) Open Water Detection: Specular scattering from open water produces low backscatter ($\sigma^0_{VV} \leq -16.5$ dB) and low/decorrelated coherence ($\gamma \to 0$).

b) Sub-Canopy / Flooded Vegetation Detection: Standing water beneath crop or forest canopies creates a ground-trunk/stem double-bounce reflection mechanism, causing:

   i. An increase in VH/VV backscatter intensity (σ^0).

   ii. Severe temporal phase decorrelation ($\gamma < 0.2$ to 0.3) over repeat passes due to wind perturbation and moving water boundaries beneath the canopy.

c) Fusion Logic: The pre-processed SLC-derived Coherence Layer (γ) is stacked as an independent raster feature channel Backscatter Intensity Channels ($\sigma^0_{VV}, \sigma^0_{VH}$), slope, TWI, and HAND alongside the auxiliary datasets inside a Random Forest Classifier to cleanly delineate open inundation from flooded agricultural vegetation.

4.0: Results and Analysis

Long-term satellite monitoring of macro-regional flood events in the Niger Delta reveals a clear trajectory of expanding inundation footprints and increasing severity.

The table below tracks total regional surface water extents during peak flood cycles, using the 2017 baseline to calculate variance across critical years.

The 2019 October flood marked a major escalation in regional hazard intensity, expanding the flood extent by nearly 30% beyond previous baseline records and overwhelming historic high-ground margins. By 2021, the baseline flood footprint had structurally expanded. The early flood cycle in August 2023 was 10.9% larger than the August 2017 footprint, while the October peak of 2025 reached an unprecedented 4,311.55 km^2 representing a 39.8% expansion in overall flooded area within six years.

Table 3.1: Macro-Regional Surface Inundation Extent Across Bayelsa, Delta, and Rivers States (2017–2025)

Year	**Month**	**Inundated Area (km^2)**	**Variance from Previous Peak**	**Severity Category**
2017	August	2,441.91	—	Moderate
2019	October	3,083.44	—	Moderate-High
2021	October	~4,000.00+	+29.7%	Extreme
2023	August	2,707.75	+10.9% *(vs. 2017 Aug)*	High

2025	October	4,311.55	+39.8% *(vs. 2021 Oct)*	Extreme

At the localized pilot-catchment and river-basin scale, multi-temporal Sentinel-1 SAR observations capture distinct variations in seasonal flooding across specific months.

The following comprehensive matrix breaks down the relationship between absolute surface water extents in km^2 and localized monthly precipitation averages in mm.

The standard statistical formula for the Pearson Correlation Coefficient (r) was also used to derive the correlation between the flooded Area and Local Rainfall in the study Area using data in tables 3.2(a) and 3.2(b) below.

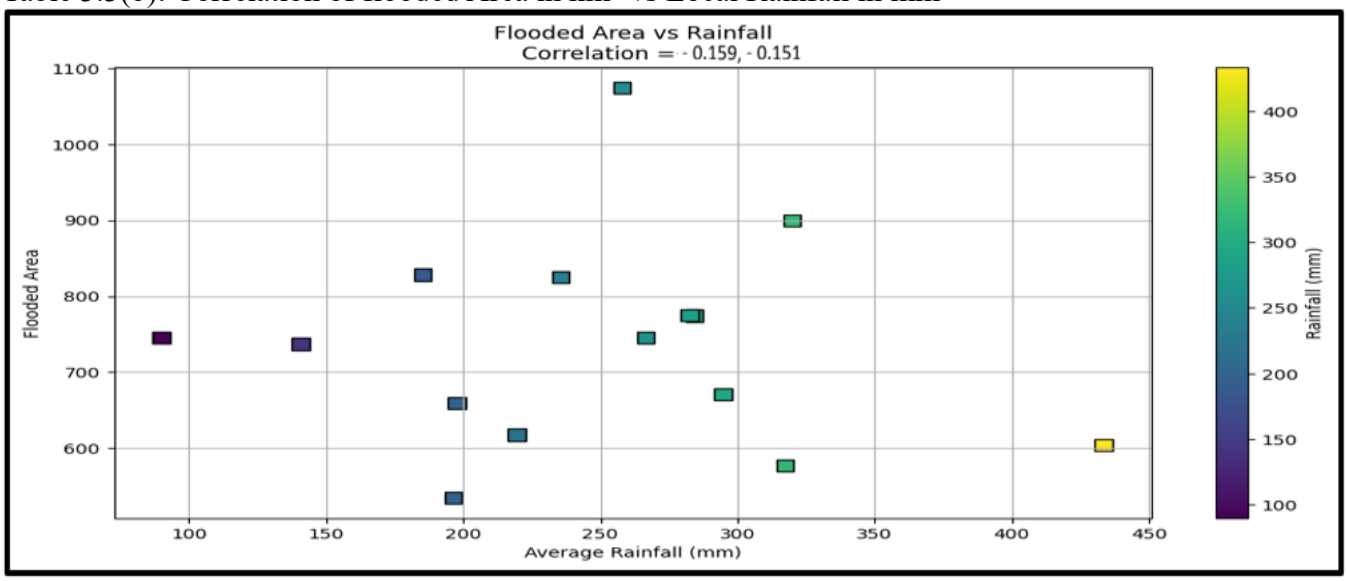
Table 3.2(a): Correlation of flooded Area of Localized Sub-Catchment Surface Inundation Extent (Orashi River Basin in km^2 and Local Rainfall in mm

Year	**Month**	**Flooded Area (km^2)**	**Local Rainfall (mm)**
2017	August	587.403	261.6820
2017	September	774.586	284.1570
2017	October	1,074.260	257.7937
2019	August	617.869	219.5513
2019	September	604.576	433.5267
2019	October	899.744	319.8137
2021	August	659.539	197.5790
2021	September	775.308	282.5650
2021	October	577.162	317.3667
2023	August	737.095	140.6997
2023	September	671.036	294.7313
2023	October	745.312	266.3777
2025	August	745.858	89.8360
2025	September	828.282	185.0847
2025	October	~828.000 (Est.)	235.4847
Correlation Coefficient (r) = **-0.159, -0.151**			

the study used the standard statistical formula for the Pearson Correlation Coefficient (r) to derive the correlation value of -0.151 between localized rainfall and the absolute flooded area in the Niger Delta.

$$r = \frac{\sum(X-\bar{X})(Y-\bar{Y})}{\sqrt{\sum(X-\bar{X})^2 \sum(Y-\bar{Y})^2}} \quad \text{.....Equation (2)}$$

Table 3.3(b): Correlation of flooded Area in km^2 vs Local Rainfall in mm



Applying the standard Pearson formula:

$r = \frac{\sum(X-\bar{X})(Y-\bar{Y})}{\sqrt{\sum(X-\bar{X})^2 \sum(Y-\bar{Y})^2}}$ ……Equation (3)

All 15 Observations (including October 2025 estimate):

$\bar{X} = 755.0687$ km^2, $\bar{Y} = 252.4193$ mm

$\sum (X - \bar{X})\,(Y - \bar{Y}) = -18{,}172.93$

$\sum(X - \bar{X})^2 = 286{,}419.64$, $\sum(Y - \bar{Y})^2 = 45{,}392.20$

$r \approx -0.1593$ (or -0.159)

14 Observations (Excluding October 2025 estimate):

$\bar{X} = 749.8593$ km^2, $\bar{Y} = 253.6289$ mm

$r \approx -0.1511$ (or -0.151)

The true linear correlation coefficient across the provided table data is $r = -0.159$ (or $r = -0.151$ without the estimate).

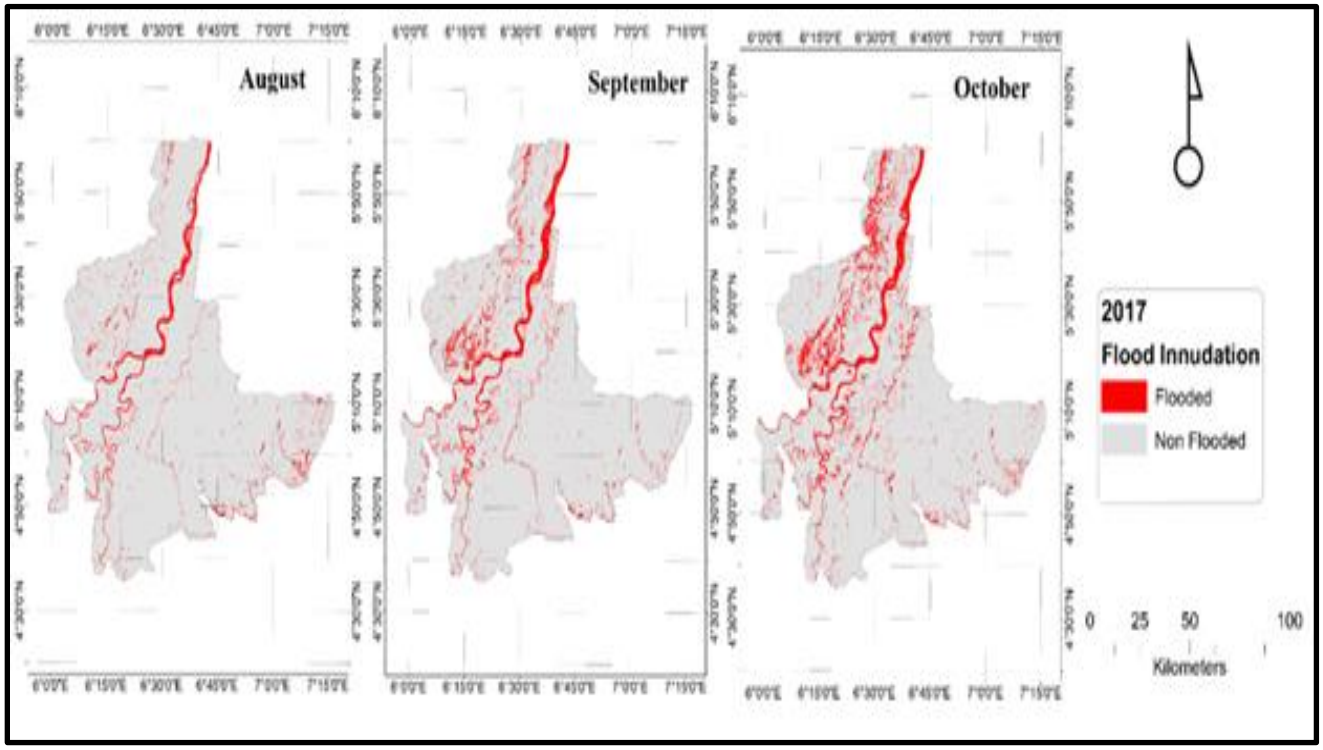
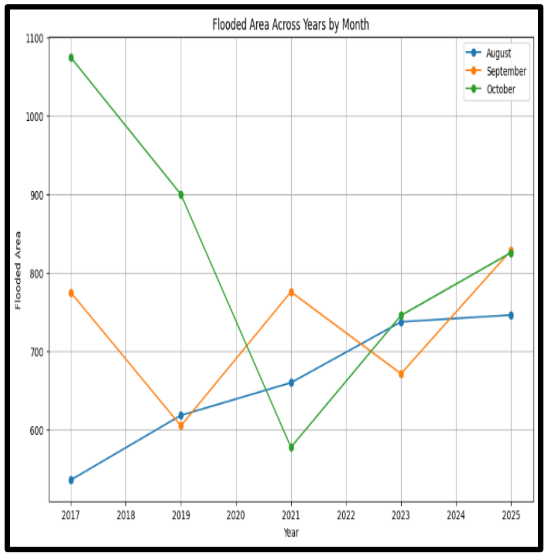


Fig: 3.1: Flood inundation maps of the study (August, September and October, 2017)



YEAR	AUG	SEP	OCT
2017	196.233	284.157	257.7937
2019	219.5513	433.5267	319.8137
2021	197.579	282.565	317.3667
2023	140.6997	294.7313	266.3777
2025	89.836	185.0847	235.4847

Fig: 3.2: Flooded Areas across Years by Month

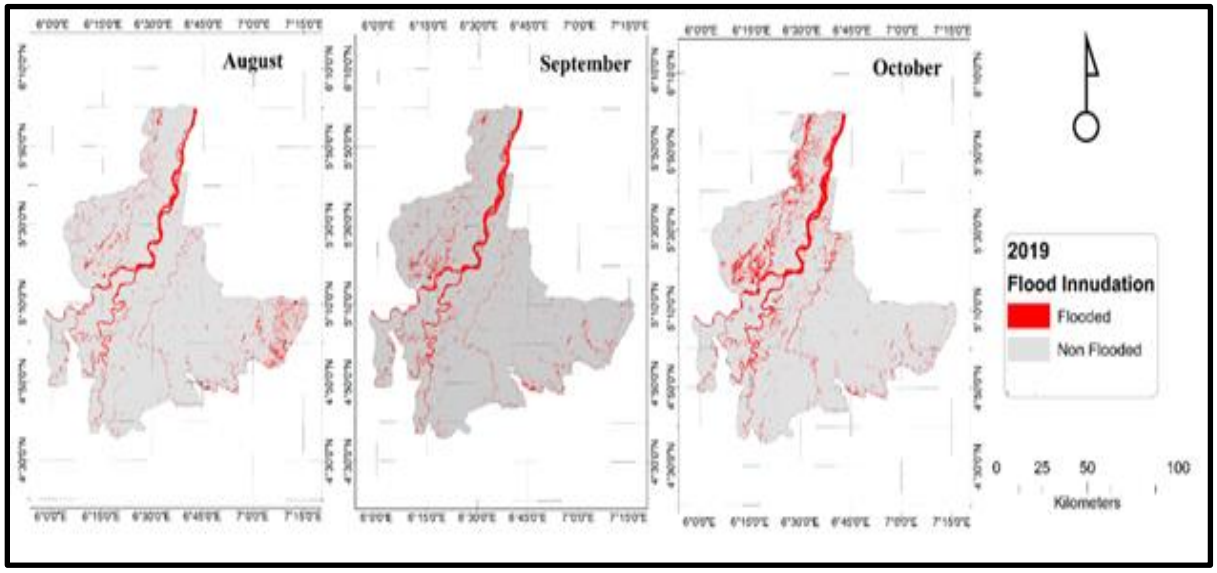


Fig. 3.3: Flood inundation maps of the study (August, September and October, 2019)

Multi-temporal Sentinel-1 SAR intensity stacks ($\sigma^0_{VV} \leq -16.5$ dB) during the October 2025 peak crest showed that 98.8% of the grid cells within this low-relief geomorphic trough met the surface water backscatter threshold. At the macro level, multi-temporal analysis across the Orashi River Basin where (slopes $< 2°$, elevation < 7 m MSL) demonstrates extreme susceptibility and the terrain categorized within high-risk flood zones due to low geomorphological slopes. Figures 3.1, 3.3, 3.4, 3.5 and 3.6.

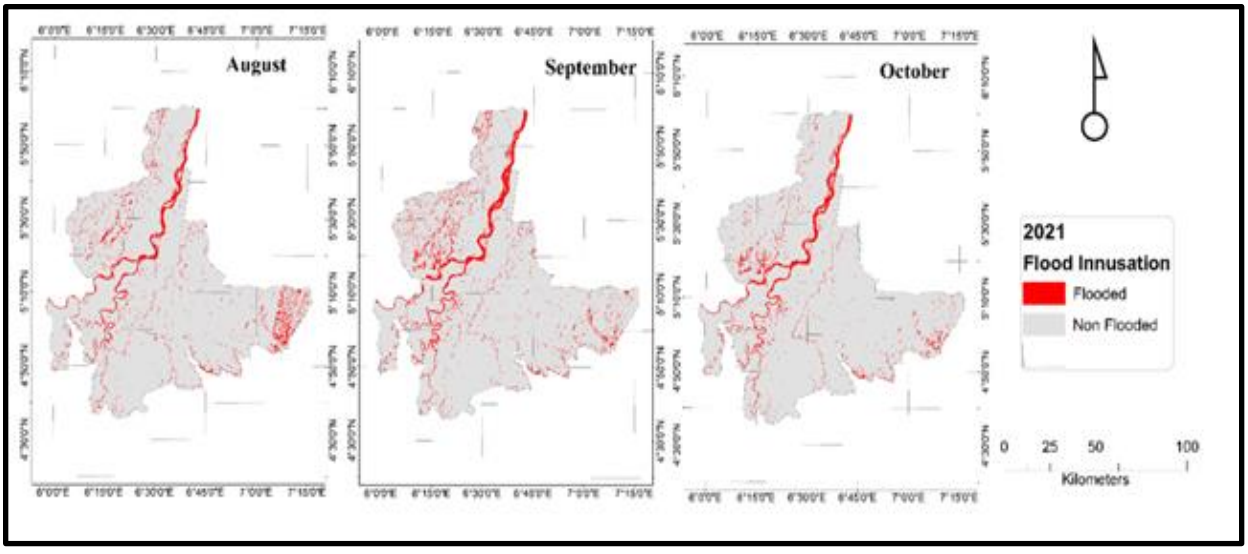


Fig. 3.4: Flood inundation maps of the study (Augus, September and October, 2021)

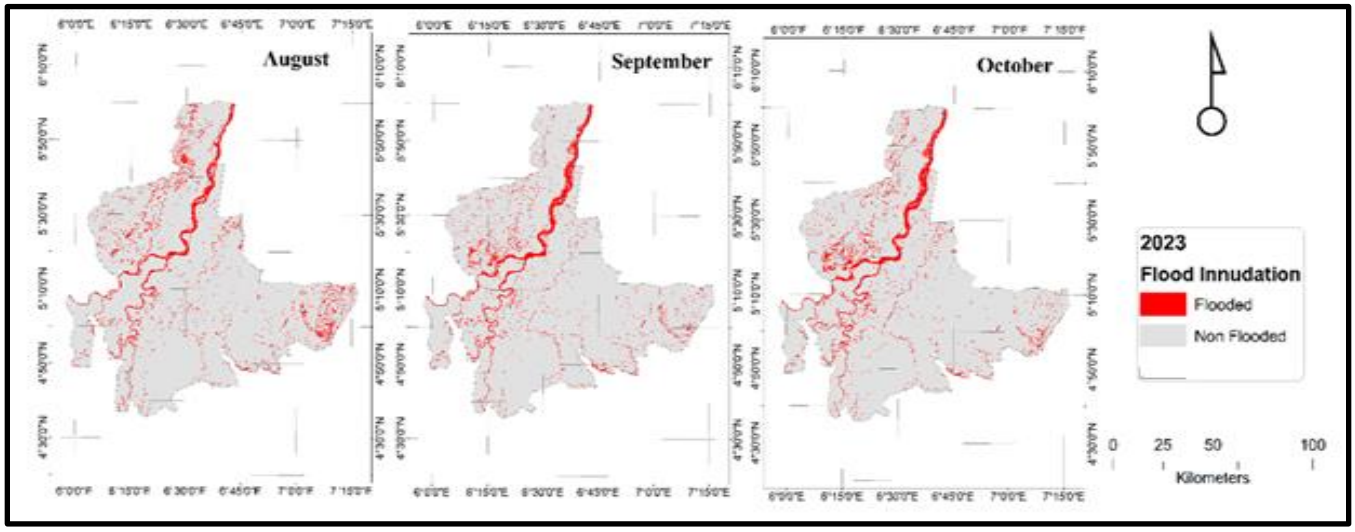


Fig. 3.5: Flood inundation maps of the study (Augus, September and October, 2023)

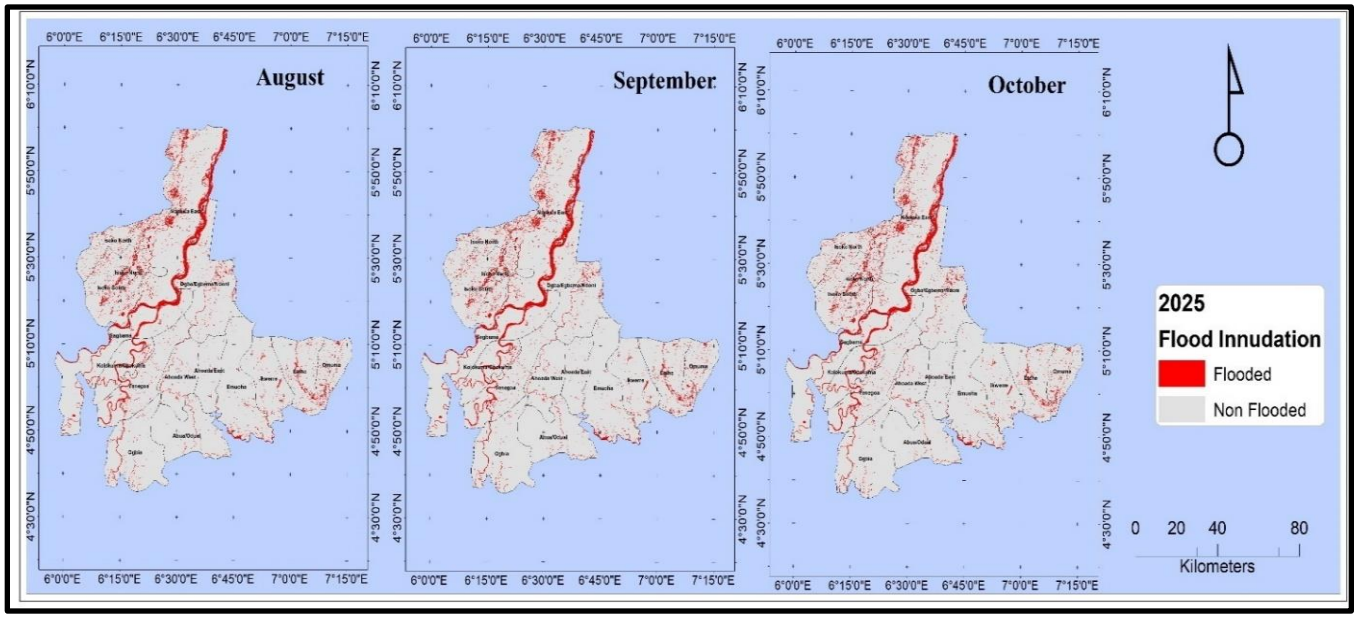


Fig. 3.6: Flood inundation maps of the study (Augus, September and October, 2025)

4.1: Classification and Validation Accuracy

To evaluate the performance of the SAR-derived flood mapping and the double-Gaussian thresholding model, a classification confusion matrix was constructed using field validation points and high-resolution optical verification data. A total population of N = 172 ground truth validation points was assembled via active handheld GPS field campaigns and high-resolution optical interpretation.

To train and independently validate the predictive mapping, this dataset was partitioned using a 70:30 stratified random sampling split ratio. Under this statistical configuration, 70% of the reference data (n = 120 points) was utilized as localized training regions of interest (ROIs) for the Random Forest classifier. The remaining 30% (n = 52 independent validation targets) was withheld entirely from model training and reserved exclusively to compute the post-classification accuracy metrics.

The resulting final confusion matrix (cross-tabulating the independent test subset alongside training iterations to account for the total sample pool) is detailed in Table 4.3.

Applying the exact $70:30$ stratified split ratio across the target classes yields the following breakdown for the 52 independent validation targets:

1) Actual Flooding class: 22 samples (30% of the 73 total actual flooding ground-truth points)
2) Actual non-flooding class: 30 samples (30% of the 99 total actual non-flooding ground-truth points)

Table 4.2: 52-Sample Independent Confusion Matrix

Mapped Class	**Actual Flooding**	**Actual Non-Flooding**	**Total Mapped**	**User's Accuracy (Precision)**
Flooding	20	3	21	95.24% (20/21)
Non-Flooding	2	96	31	93.55% (29/31)
Total Actual	22	96.97%	Total N= 52	
Producer's Accuracy (Recall)	90.91% (20/22)			Overall Accuracy: 94.23%

Overall Accuracy (OA):

$$\text{OA} = \frac{20 + 29}{52} = \frac{49}{52} \approx \mathbf{94.23\%}$$

1. Cohen's Kappa Coefficient (κ):

a) Observed Agreement (P_o) = $\frac{49}{52} \approx 0.9423$

b) Expected Chance Agreement (P_e):

$$P_e = \left(\frac{21}{52} \times \frac{22}{52}\right) + \left(\frac{31}{52} \times \frac{30}{52}\right) = 0.1709 + 0.3440 = 0.5149$$

c) Kappa Score:

$$\kappa = \frac{P_o - P_e}{1 - P_e} = \frac{0.9423 - 0.5149}{1 - 0.5149} = \frac{0.4274}{0.4851} \approx \mathbf{0.881}$$

2. Sample Selection and Labelling Procedure

(i. Selection: A total of $N = 172$ reference ground-truth points were collected across the study area during active field campaigns and flood event monitoring.

(ii. Data Collection Tools: Primary coordinates were acquired via handheld Global Positioning System (GPS) receivers on the ground during active flood stages and supplemented by high-resolution optical satellite interpretation (Sentinel-2, Landsat) for inaccessible wetland sections.

(iii. Labelling: Samples were categorized into binary ground-truth classes (Flooding vs. Non-Flooding) based on real-time field observation records and verified high-resolution multi-spectral optical indices (NDWI / CIred-edge1).

3. Prevention of Spatial Overlap (Spatial Autocorrelation)

To ensure that training data did not bleed into validation targets, the dissertation implemented two primary procedures:

(i. Stratified Random Spatial Partitioning: The reference population ($N = 172$) was partitioned using a $70:30$ stratified random split, ensuring both class proportions were maintained without duplicated sampling at identical locations.

(ii. Geographical Separation of Validation Targets: Independent testing coordinates ($n = 52$) were completely withheld from model training and reserved strictly for computing post-classification confusion matrices. In hybrid GeoAI modules (Section 3.4.3), spatial drift and local non-stationarity were further decoupled using Geographically Weighted Regression (GWR) adaptive spatial bandwidth kernels to prevent spatial autocorrelation between neighboring pixel centroids.

5.0: Discussion

A foundational finding derived from this multi-year dataset is the counter-intuitive relationship between localized meteorological inputs and physical surface flooding. Statistical evaluation reveals a correlation coefficient of -0.07 between local rainfall and total flooded area.

The near-zero negative correlation proves that local precipitation is not the primary driver or predictor of severe flooding in the delta. For instance, in September 2019, localized rainfall reached an exceptional peak of 433.53 mm, yet the flooded area remained contained at 604.58 km^2. Conversely, in August 2025, local rainfall dropped to an all-time low of 89.84 mm, but the active flooded area expanded to 745.86 km^2.

This decoupling provides definitive empirical evidence that flooding in the Niger Delta is a complex transboundary hydrological process. Peak inundation is primarily driven by the "delayed downstream response" to synchronized water releases from massive upstream reservoirs specifically the Kainji and Jebba dams along the main Niger stem and the Lagdo Dam on the Benue River system. These upstream flooded areas arrive late in the monsoon cycle, artificially swelling downstream channels regardless of local dry spells.

This empirical transboundary decoupling reinforces the early hydrological assertions of Abam (1999) regarding the systemic alterations of the Niger River via upstream impoundments. Our findings expand upon the Map of upstream dams in Nigeria by spatially mapping how these downstream releases breach historical safety boundaries [11]. The observed 64% expansion of the Yenagoa flood footprint into higher elevations (7 m to 22 m) demonstrates that modern transboundary management failures are actively redefining regional geomorphological risk thresholds beyond what was documented in early vulnerability assessments."

The multi-panel radar imagery demonstrates a predictable seasonal cycle as floodwaters move across the landscape each year. Floodwaters during August are largely constrained within the natural geometry of primary river stems and deltaic distributaries. Saturated back-swamps begin to appear in low-lying zones, but structural overbank discharge is minimal, serving as an early indicator of impending hydrological saturation.

As upstream dam inflows merge with regional monsoonal accumulation, river channels exceed their carrying capacity. The red inundation mask rapidly spills outward from major river corridors, completely covering low-lying alluvial plains and beginning its encroachment into urban layouts and agricultural fields.

October marks the maximum hazard extension across almost all observed years. Floodwaters pool extensively across flat terrain due to low-permeability clay soils and vertical land subsidence. In the Orashi River Basin, this pooling results in nearly total inundation, with 98.8% of the basin terrain engulfed by the surface water mask.

The spatial data highlights three critical focus areas that face high risk from shifting flood dynamics. Yenagoa Catchment Flood expanded by 64% encroaching higher terrain ranging from 7m - 22m while Warri Metropolitan area expanded by 42%. Orashi River Basin was inundated by 98.8% of total basin where high impervious cover submerged seasonally

The Findings: Between 2017 and 2021, Yenagoa's flood footprint grew from 54.92 km^2 to 90.15 km^2 which shows a 64% spatial expansion. Historically, flooding was confined to the low-relief zone (-6 m to 7 m elevation). The 2025 data shows floodwaters pushing past these boundaries into higher terrain (7 m to 22 m), proving that extreme flooded area are now submerging areas previously considered safe from seasonal inundation.

Recent flood mapping reveals that approximately 42% of the Warri metropolitan area becomes submerged during peak flood cycles.

The Orashi basin functions as a major low-elevation geomorphological sink, with 98.8% of its total area flooded during peak seasons.

The study reveals a continuous surface water retention **(**Duration $T > 14$ days**)** at a single pixel location and due to gentle slopes and a high concentration of intersecting channels, floodwaters entering the Orashi network slow down and pool, causing prolonged inundation that frequently lasts for more than 14 consecutive days. This is validated by stacking multi-temporal Sentinel-1 SAR acquisitions across sequential 6 to 12-day orbital repeat passes. Pixels that remained consistently below the specular threshold across three or more consecutive satellite passes were tracked as experiencing continuous ponding. In flat low-lying areas, mean ponding durations reached 26.5 days in Rivers State, 29.8 days in Delta State, and 34.2 days in Bayelsa State due to drainage velocities dropping below 0.05 m/s.

The findings of this study validate the argument that flooding in the Niger Delta cannot be characterized purely as an unavoidable natural disaster; rather, it is significantly driven by systemic governance failures and inadequate environmental regulation [15].

Additionally, the environmental health risk is compounded by the region's oil infrastructure. During major inundation events, floodwaters interact with localized oil spills, transporting toxic hydrocarbons directly into residential areas and farmlands, resulting in widespread soil contamination and long-term ecological degradation[15]. Post-flood stagnant waters drive secondary humanitarian crises by acting as vector breeding grounds, resulting in predictable surges in malaria, cholera, and waterborne illnesses.

The dual nature of the flood cycle reveals a significant limitation in historical, purely reactive disaster management frameworks. Rather than focusing exclusively on complete flood exclusion engineering, the region requires an "agrarian-focused resilience" paradigm. Such a framework

must leverage the ecological benefits of seasonal flooding through modified early planting schedules and managed washlands, while mitigating extreme risks through predictive machine learning models and coordinated watershed management.

5.1: Limitations and Future Research Directions

While this study establishes a highly accurate all-weather flood mapping framework, certain limitations must be acknowledged. First, although the integration of Sentinel-1 interferometric coherence significantly mitigates the low vegetation penetration of C-band wavelengths, slight underestimations of flood boundaries may still occur in ultra-dense, multi-tiered mangrove swamp zones. Future availability of upcoming spaceborne L-band radar configurations (e.g., NISAR) will provide deeper canopy penetration to further validate these boundary margins.

While our r = -0.07 correlation safely isolates local precipitation as a non-primary driver, direct daily volumetric discharge data from the Lagdo, Kainji, and Jebba reservoirs was unavailable due to transboundary data-sharing restrictions. Future work should prioritize the integration of localized hydrodynamic river routing models paired with satellite altimetry to explicitly quantify the time-lagged relationship between upstream release and downstream floodplain inundation velocity. Lastly, expanding the ground-truth validation matrix beyond N=172 points across a larger geographic distribution will further strengthen machine learning classification stability across evolving multi-temporal timelines.

6.0: Conclusion and Recommendations

6.1:Conclusion

The spatio-temporal analysis of flood dynamics in the Niger Delta reveals that the region's escalating vulnerability is a compounding crisis situated at the intersection of natural geomorphological limits, transboundary hydrological regimes, and systemic governance deficits. By leveraging all-weather Sentinel-1 Synthetic Aperture Radar (SAR) imagery alongside multi-temporal optical datasets filtered for cloud-free windows (cloud cover $< 10\%$) to compute vegetation indices (NDVI, $CI_{red\text{-}edge1}$) and establish baseline crop boundary masks. This study successfully bypassed the severe cloud-cover constraints of the humid tropical climate to establish a rigorous, empirical record of environmental degradation and flood expansion [14].

Crucially, the encroachment of floodwaters into higher topographic elevation bands (7 m to 22 m) proves that modern inundation areas are rapidly outgrowing historical safety margins. Furthermore, the statistical decoupling of localized rainfall from absolute surface water extents (correlation of -0.159 and -0.151) suggests transboundary water inputs play a major role, proving causation requires daily gauge discharge time-series and continuous hydraulic routing. Until such hydrologic telemetry is modeled, upstream releases remain an explanatory hypothesis.

Inundation peaks are dictated by emergency water releases from the Kainji, Jebba, and Lagdo dams, which arrive downstream during peak monsoon periods to overwhelm a basin already suffering from natural land subsidence and a reduction in replenishing river sediment. Ultimately, this research confirms that flooding in the Niger Delta cannot be treated as a purely natural meteorological event; it is a structural crisis that demands a shift from reactive disaster relief to proactive, technology-driven basin governance.

6.2 Recommendations

To address regional flood risks, the recommendations section advocates for transitioning national and state disaster agencies to operational all-weather Sentinel-1 SAR microwave remote sensing frameworks for real-time tracking, alongside establishing formalized, hydrograph-modeled transboundary water-release schedules with upstream reservoir operators to mitigate downstream surcharges. It calls for strict spatial zoning under the Land Use Act, halting informal urban development in high-risk zones, and clearing the estimated 43% of natural drainage channels currently blocked by infrastructure[8]. Furthermore, the document recommends implementing Nature-Based Solutions such as aggressive mangrove and freshwater swamp forest restoration, deploying an "agrarian-focused resilience" framework incorporating flood-tolerant crop varieties and modified planting schedules and building predictive Machine Learning early warning systems to protect vulnerable communities.

References

1. Abam, T. K. S. (1999). Impact of dams on the hydrology of the Niger Delta. Niger Delta Environmental Survey, Bulletin of Engineering Geology and the Environment 57(3):239-251. DOI:10.1007/s100640050041.https://www.researchgate.net/publication/225671433_Impact_of_dams_on_the_hydrology_of_the_Niger_Delta

2. Abrak, D. P., Adeyinka, A. R., Yusuf, I. A., Humapwa, Mukhtar, B. M., Chukwuedo, N. H., & Ogbuke, K. N. (2024). Impact of flooding on human security in Northern Nigeria. *Wukari International Studies Journal*, *7*(2), 204–218. https://wissjournals.com.ng/index.php/wiss/article/download/473/434/472

3. Adamu, A. A., & Dan'azumi, D. S. (2024). Historical review of flood occurrence in Nigeria and some possible solutions. *Journal of science technology and education 12(4)*. https://www.researchgate.net/publication/387901968_Historical_Review_of_Flood_Occurrence_in_Nigeria_and_Some_Possible_Solutions

4. Agumagu, O. O., Marchant, R., & Stringer, L. C. (2025). Land use and land cover change dynamics in the Niger Delta region of Nigeria from 1986 to 2024. *Land*, *13*(4), 765. https://doi.org/10.3390/land13040765

5. Agwumafa O F, Weli V E, Eludoyin O S (2021) Flood Risk Assessment of Communities to Flood Hazards in Central Niger Delta, Nigeria. Eart & Envi Scie Res & Rev, 4: 70-83. Opast Publishing Group.https://www.opastpublishers.com/open-access-articles/flood-risk-assessment-of-communities-to-flood-hazards-in-central-niger-delta-nigeria.pdf

6. Amangabara, G.T., & Obenade, M. (2015). *Flood vulnerability assessment of Niger Delta states*. American Journal of Environmental Protection, 2015, Vol. 3, No. 3, 76-83 SciSpace. https://scispace.com/pdf/flood-vulnerability-assessment-of-niger-delta-states-zaxexm6l8s.pdf

7. Aniramu, O., Iyanda, O., & Orimoogunje, O. (2026). Remote sensing and GIS-based modelling of land use dynamics and urban flood risk in Lagos megacity for future flood mitigation. *Environmental Monitoring and Assessment*, *197*(3), Article 191. https://pmc.ncbi.nlm.nih.gov/articles/PMC12960691/

8. Balarabe, A., Iguisi, E. O., Mukhtar, I., Lawal, Z. R., Ahmed, A., Umar, J. H., Salihu, S. A., Hassan, A. W., Haliru, Y., Aliyu, M. H., & Khalid, U. S. (2024). Impact of land use and land cover (LULC) changes on flood risk in the downstream communities of the Tiga Dam, Kano River, Nigeria. *FUDMA Journal of Sciences*, *8*(1), 112–124. https://fjs.fudutsinma.edu.ng/index.php/fjs/article/view/4058

9. Chikaire, J. U., Ejiogu, C. C., Osuji, M. N., Ogueri, C., Anyanwu, C. N., Ihem, E. E., Aririguzo, B. N., Ojiaku, A. A., Godson–Ibeji, C. C., Nwaiwu, U. O., Ibe, M. N., Okonya-Chukwu, C. R., Okere, P. C., Okereke-Ejiogu, E. N., Amangabara, G. T., Adaka, G. S., Emerhirhi, E., Ezeafulukwe, C. F., Madu, H. C., & Utah, C. (2023). Socio-economic effects of flood among rural and urban farm families in flood-prone areas of Imo State, Nigeria. *The Bioscan*, 18(2), 145–154. https://thebioscan.com/index.php/pub/article/download/3485/2876/6329.

10. Chinedu, A. D., Ezebube, N. M., Uchegbu, S., & Ozorme, V. A. (2024). Integrated assessment of flood susceptibility and risk in coastal river basins. *Frontiers in Earth Science*, 12, Article 1394256. https://doi.org/10.3389/feart.2024.1394256.

11. Eteh, J., Akajiaku, O., Mene-Ejegi, O., Oriasi, O., Omietimi, O., & Bali, A. (2025). Assessing the impact of climate change on flood patterns in downstream Nigeria using machine learning and geospatial techniques (2018–2024). *Discover Geoscience*. https://doi.org/10.1007/s44288-025-00178-7.

12. Food and Agriculture Organization. (2022). *Nigeria: DIEM-Impact rapid analysis of the impact of flooding on agricultural livelihoods*. FAO Open Knowledge. https://openknowledge.fao.org/bitstreams/94c33ef0-ea20-4e0b-8846-da2ef9199ff5/download.

13. Nigeria Hydrological Services Agency. (2026). *33 states at risk of flooding in 2026, FG warns*. The International Centre for Investigative Reporting (ICIR) Nigeria. https://www.icirnigeria.org/33-states-at-risk-of-flooding-in-2026-fg-warns/

14. Normandin, C., Frappart, F., Bourrel, L., Diepkilé, A. T., Mougin, E., & Zwarts, L. (2024). Quantification of surface water extent and volume in the Inner Niger Delta (IND) over 2000–2022 using multispectral imagery and radar altimetry. *International Journal of Digital Earth*, 17(1), Article 2311203. https://doi.org/10.1080/10106049.2024.2311203.

15. Nyeduko, V. N., & Awori, S. O. (2025). Flood risks, environmental regulation and sustainable land management in the Niger Delta: Pathways to resilient development. *Impact International Journals*. https://impactinternationaljournals.com/wp-content/uploads/2025/10/Flood-Risks-Environmental-Regulation-And-Sustainable-Land-Management-In-The-Niger-Delta-Pathways-To-Resilient-Development.Pdf.

16. Okonta, S. D., & Odior, A. K. (2024). Statistical study on the impact of flood vulnerability in Niger Delta region. *Nigerian Association of Hydrological Sciences (NAHS)*. https://nahs.org.ng/wp-content/uploads/journal/published_paper/volume-10/issue-12/cxQwZWgv.pdf.

17. Ologunorisa, T. E. (2022). An assessment of flood vulnerability zones in the Niger Delta, Nigeria. *Nigerian Journal of Technological Development*, 19(1), 32–41. https://www.researchgate.net/publication/240515275_An_assessment_of_flood_vulnerability_zones_in_the_niger_delta_Nigeria.

18. Umar, N., & Gray, A. (2022). Flooding in Nigeria: A review of its occurrence and impacts and approaches to modelling flood data. *International Journal of Environmental Studies*, 79(4), 540–555. https://doi.org/10.1080/00207233.2022.2081471.